Balanced restoration of geological volumes with relaxed meshing constraints ☆

Pauline Durand-Riard[a,*,1], Guillaume Caumon[a], Pierre Muron[a,b]

[a] *Centre de Recherches Pétrographiques et Géochimiques - CNRS, School of Geoloy, Nancy-Université, Rue du doyen Marcel Roubault, 54501 Vandoeuvre-lès-Nancy, France*
[b] *Chevron ETC, 6001 Bollinger Canyon Rd., San Ramon, CA 94583, U.S.A.*

Abstract

Balanced restoration consists in removing the effects of tectonic deformation in order to recover the depositional state of sedimentary layers. Restoration thus helps in the understanding of a geodynamic scenario, reduces structural uncertainties by testing the consistency of the structural model, and, under mechanical behavior assumptions, evaluates retro-deformation. We show how an elastic finite element model can be used to solve restoration problems, by setting displacement boundary conditions on the top horizon and contact boundary conditions on the fault cut-offs. This method is generally applied on a tetrahedral mesh, which raises significant meshing problems in complex structural settings, where restoration is particularly useful. Indeed, the mesh has to be conformable to both faults and horizons, including unconformities and onlap surfaces, which may drastically increase the number of elements and decrease the mesh quality. As an alternative, we propose to represent unfaulted horizons as a property of the tetrahedral model, and to transfer the associated boundary conditions onto the neighboring nodes of the mesh, using an "implicit" approach. The proposed methods are demonstrated on a typical example and results show good agreement between both approaches. While the computational time is equivalent in both cases, the time needed for model building is significantly reduced in the implicit case. In addition, the implicit method provides a convenient way to handle unconformities in restoration, both for eroded surfaces, and on onlap layer geometries. In such cases, our method provides a flexible way to specify the amount of eroded material, and generates less mesh elements than the conforming mesh, thereby reducing computational time.

Key words: Structural geology, balanced restoration, geomechanics, implicit

☆ Published as Computers and Geosciences 36(4):441–452. DOI:10.1016/j.cageo.2009.07.007

* Corresponding author

Email addresses: durandriard@gocad.org (Pauline Durand-Riard), Guillaume.Caumon@ensg.inpl-nancy.fr (Guillaume Caumon), pimu@chevron.com (Pierre Muron), (Pierre Muron)

[1] Phone number: +333 83 59 64 50; fax number: +333 83 59 64 60

Introduction

Three dimensional (3D) geometrical interpretation of geological structures from subsurface data is often poorly constrained, and hence needs to be checked for consistency. Balanced restoration, which aims at unfolding and unfaulting a stack of layers, provides unique insights in this regard. In particular, restoration can reduce structural uncertainties by testing the model consistency, quantifying extension/shortening and deformation, and validating interpretations. The simplest structural restoration techniques are based upon geometric constraints and implemented on cross-sections and maps. Typically, conservation of length in the shear direction, or conservation of area, length and angle have been proposed (Dahlstrom, 1969; Gibbs, 1983; Gratier and Guillier, 1993; Rouby, 1994; Rouby et al., 2000). However, in complex 3D domains, tectonic deformation can hardly be simplified to plane strain or simple shear, and hence should be addressed with a true volumetric approach. To achieve 3D restoration, several authors have proposed to replace traditional geometric assumptions by geomechanical principles (De Santi et al., 2002; Maerten and Maerten, 2006; Massot, 2002; Moretti, 2008; Moretti et al., 2006; Muron, 2005). In this case, restoration is formulated as a finite element problem, usually using a piecewise isotropic linear elastic material and setting appropriate boundary conditions. The practical implementation of such a model requires generating well-shaped finite-element meshes conforming to all geological surfaces (horizons and faults). To-date, such a finite element mesh may consist of a corner-point hexahedral grid (stratigraphic grid) used in most flow simulation codes, or a tetrahedral mesh. Stratigraphic grids often introduce stair-stepped faults and rectilinear pillars. We believe such simplifications are seldom acceptable in complex structural models for which restoration is most useful. Therefore, we propose, as most authors (De Santi et al., 2002; Moretti, 2008; Muron, 2005) to work on restoration formulated on tetrahedral meshes, for they provide the necessary flexibility to accurately represent complex structural domains (Section 1). The main practical limitation of restoration on tetrahedral meshes often lies in the generation of a conforming mesh. Indeed, building a mesh conforming to both faults and stratigraphic boundaries raises tremendous difficulties in maintaining a satisfactory shape of mesh elements (Owen, 1998). In particular, unconformities are not only difficult to mesh but also significantly increase the number of elements, which slows down computations. In this paper, we restore stratigraphic models with relaxed meshing constraints. For this, we consider horizons as isovalue surfaces of one or several scalar property(ies) represented on the volume of interest (Fig. 3). These implicit horizons can be computed from scattered data as described by Frank et al. (2007). This new implicit approach relies on new boundary conditions and the new definition of rock properties (Section 2). An application of the explicit and implicit formulations is used to compare results (Section 3), and the implicit restoration is demonstrated on unconformities (Section 4).

1. Goals and methods of balanced restoration

1.1. Principle

A deformed sedimentary succession can be returned to its original depositional state by removing the effects of tectonic forces. This balanced restoration process aims at reducing the uncertainties and testing the model's consistency: the restoration properties, such as dilation or eigen values and vectors of the strain tensor, can be computed and provide information about the spatial distribution of deformation. This insight can then lead to the identification of inconsistent zones, where interpretations may be wrong. When interpretations are deemed correct, restoration and derived strain distribution analysis also provides information about location and orientation of fractures, which are more realistic than the use of horizon curvatures.

Restoration was first conceived by Chamberlin (1910) on cross sections, and then formalized by Dahlstrom (1969). More recently, this process has been extended to maps (Dunbar and Cook, 2003; Gibbs, 1983; Gratier and Guillier, 1993; Jacquemin, 1999; Massot, 2002; Rouby, 1994; Rouby et al., 2000; Thibert et al., 2005) and volumes (De Santi et al., 2002; Moretti et al., 2006; Muron and Mallet, 2003). The method restores sedimentary layer boundaries to their original geometry, assuming they were continuous and horizontal. Restoration rules are based on geometric criteria, considering:

a) shear deformation (vertical or inclined): lengths are conserved along the shear direction (Gibbs, 1983; Rouby et al., 2000). Fault restoration can be performed by rigid block rotations (Gratier and Guillier, 1993; Rouby, 1994);
b) flexural slip deformation: areas are preserved (Dahlstrom, 1969; Rouby et al., 2000) and faults can be closed by setting constraints on fault borders to compute a parameterization on the surface (Massot, 2002; Thibert et al., 2005).

Restoration can be done sequentially (Fig. 1): once the uppermost layer is restored, it is removed (backstripping). This helps to assess ongoing deformation or several deformation phases recorded by depositional processes (growth stratigraphy).

In three dimensions, geometric restoration algorithms cannot be simply implemented: with the classical assumptions, the restoration problem would be underconstrained and several deformation paths would be possible. Since we don't know the deformation path and consider the different tectonic events as one single event (or several events recorded in syntectonic sediments), we need to have one reversible path. A simple geometric assumption is made on volume preservation but other assumptions are needed to find a unique solution to this problem. Additionaly, rock heterogeneity is an important parameter in the distribution of strain. For these reasons, it has been proposed to turn the unfolding problem into a geomechanical problem (De Santi et al., 2002; Dunbar and Cook, 2003; Moretti et al., 2006; Muron and Mallet, 2003). The first step is then to define a mesh conforming to the geological interfaces (faults and

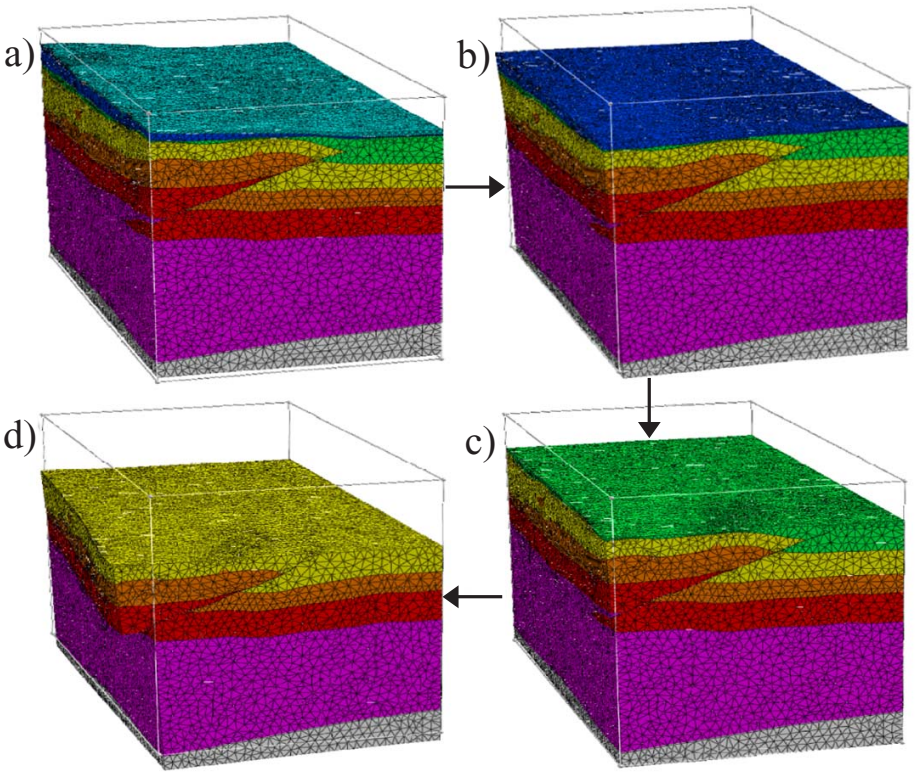

Figure 1: Example of balanced restoration on a fault-propagation fold model: a) is the initial model; b) is the first restored sequence: the topmost horizon of the blue layer has been restored and the light blue layer has been removed; c) is the second restored sequence: the upper horizon of the green layer has been restored and the blue layer has been removed; d) is the third restored sequence: the topmost horizon of the yellow layer has been restored and the green layer has been removed. Model courtesy of Harvard University and Chevron, restored using RestorationLab in Gocad. From Muron (2005).

horizons), associate mechanical properties to rock units, and then apply some boundary conditions.

1.2. Boundary conditions

Boundary conditions are applied to the structural model to constrain the calculated restoration pathway. In most approaches, they are applied onto a discrete mesh, by specifying the original elevation of the restored horizon and by fixing specific mesh elements in space (Dirichlet conditions, see Fig. 2):

a) Geometry of the reference horizon - This condition is usually applied to the topmost geologic layer; it reflects the assumption made on its geometry at the time of deposition (e.g., Groshong, 1999, chap. 11): most of the time, a flat datum is specified at a given reference elevation Z_r :

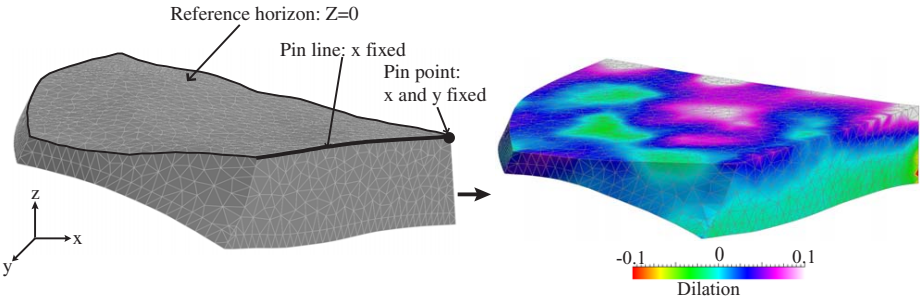

Figure 2: The following boundary conditions are applied to the initial model (left) to obtain the restored model (right): the topmost horizon is set to a reference elevation $z = 0$; a pin point is fixed along the axis x and y and a pin line along the x axis. The retrodeformation, computed from the deformations between the current configuration and the restored one, is painted on the restored solid.

$$Z(n) = Zr$$

Where $Z(n)$ is the elevation of a node n in the restored state.

b) Location of fixed elements - It is necessary to specify part of the domain as fixed, either to ensure the existence of the solution, or for practical interpretation reasons (e.g., Groshong, 1999, chap. 11): this can be a single point (pin point), a boundary of a block (pin wall or line), or an entire block (pin block). In practice, one or more components are fixed during restoration:

$$X_i(n) = x_i(n)$$

Where x_i is the i^{th} coordinate of the node n to be fixed, and X_i its coordinate in the restored state.

Algorithms to set these boundary condiditions are available in Appendix A. If the model contains faults, some additional conditions are necessary to minimize gaps and overlaps in the restored state. In this paper, we consider only folded structures; details about fault compliance conditions are described by Wriggers (2000) and Muron (2005).

1.3. Restoration as a geomechanical problem

The boundary conditions constrain the target restored geometry for a subset of the model. Several authors suggest using continuum mechanics to reach a solution that has physical sense, and that can reflect known mechanical heterogeneities (De Santi et al., 2002; Dunbar and Cook, 2003; Maerten and Maerten, 2006; Moretti et al., 2006; Muron and Mallet, 2003). This formulation uses conservation of mass and of linear momentum, as described in Appendix B. In this mechanical formulation, homogeneous and isotropic elastic rock behavior is often assumed. This material behavior follows the generalized Hooke's law,

which states that the components of the stress tensor σ_{ij} are linearly related to the components of the strain tensor ε_{ij}:

$$\sigma_{ij} = \lambda \cdot \delta_{ij} \cdot e + 2\mu \cdot \varepsilon_{ij} \qquad \forall (i,j) \in \{x,y,z\} \tag{1}$$
$$\text{with:} \qquad e = (\varepsilon_{xx} + \varepsilon_{yy} + \varepsilon_{zz}) = trace(\varepsilon)$$

where λ and μ are the Lamé parameters, and δ_{ij} is the Kronecker's symbol equal to 1 if $i = j$ and 0 otherwise.

In subsurface geological models, mechanical properties such as Lamé parameters are available either from lithology or from petroelastic inversion of seismic data (Doyen, 2007). In the case of properties obtained from lithology, values are computed through laboratory tests and may actually be very different from real rock behavior at a larger scale (Titeux and Royer, 2008). Moreover, elastic behavior remains a simplifying assumption because geomechanical variables vary through times and rock deformation mechanisms are clearly elastoplastic or viscoplastic, and include compaction (Charlez, 1991; Sheider et al., 1996). Unfortunately, such rheologies are not applicable to restoration since they are not implied in reversible phenomena (Moretti et al., 2006). Moreover, their application calls for stress boundary conditions through time, which are often unknown throughout geologic time. Therefore, to simplify the problem and for practicality, we use linear elastic behavior for restoration. To-date, the effect of these simplifications is subject to active research, and discussions may be found in Moretti (2008) and Guzofski et al. (2009).

Once the boundary conditions have been set (Algorithms 1 and 2 in Appendix A), the geomechanical statements make up a well-posed problem. The numerical resolution of this problem can be performed using the Finite Element Method using the variational approach (Hugues, 1987; Zienkiewicz, 1977; Zienkiewicz and Taylor, 2000a,b).

1.4. Practical limitations

The approach described above is seldom applied to subsurface studies (Guzofski, 2007; Guzofski et al., 2009; Plesch et al., 2007). This can be partly explained by the detailed subsurface modeling knowledge required by geologists to build 3D structural models. In any case, generating a conforming mesh itself is particularly challenging in the case of complex structural models. In this work, we use the Delaunay-based tetrahedral meshing method described by Lepage (2002), and the macro-topological model of Muron (2005), which attaches information about geological interfaces to tetrahedral mesh boundaries.

However, conforming mesh generation is known to be very challenging in the case of dense constraints (Lo, 2002; Owen, 1998), which occur in densely faulted domains and in thin or pinched out layers. In these cases, mesh generation is difficult, requiring time-consuming interactive input and quality control. Moreover, a very large number of elements is necessary to ensure sufficient mesh quality for the success of finite element computations. Such a mesh refinement has a high computational cost; meshing algorithms may even fail to maintain a

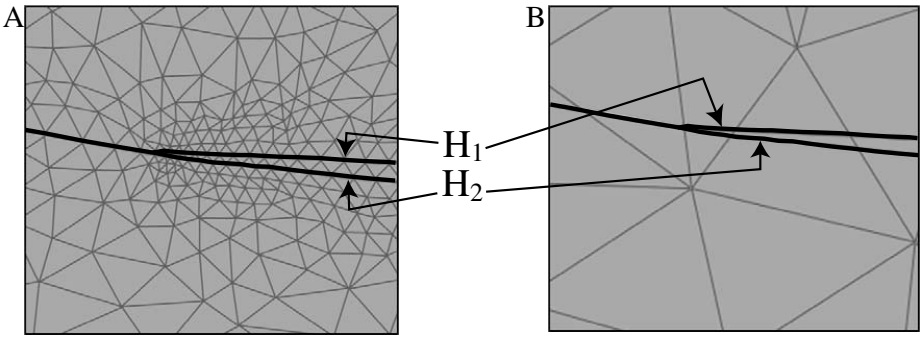

Figure 3: The picture A shows a mesh conforming to the horizons H_1 and H_2 as required for the explicit approach; picture B shows a model with an implicit approach: the mesh is not conformable to the horizons. The mesh complexity increases when the horizon pinches out.

good element shape, when conforming surfaces are too close or too dense, due to limited computer precision (Owen, 1998). This leads us to develop a method where we can relax meshing constraints without introducing geometrical simplifications, to simplify the restoration process.

2. Relaxing meshing constraints

2.1. Defining horizons as scalar fields

While explicit structural modeling methods require the construction of fault and horizon surfaces to define a structural framework, implicit methods consider geological interfaces as iso-surfaces of a 3D scalar field. Calcagno et al. (2008); Caumon et al. (2007); Frank et al. (2007); Moyen et al. (2004) used this approach and proposed the representation of the horizons with one or several properties interpolated over a mesh. This property may have a chronostratigraphic significance (Mallet, 2004; Moyen et al., 2004), or may be defined more generally as some scalar potential or distance field (Calcagno et al., 2008; Caumon et al., 2007; Frank et al., 2007). In this work, a horizon corresponds to a property iso-value on a tetrahedral mesh (Fig. 3). The property on this tetrahedral mesh can be computed from available subsurface data by Discrete Smooth Interpolation (Caumon et al., 2007; Frank et al., 2007; Mallet, 1992) or dual kriging with a discontinuous drift (Calcagno et al., 2008). Typically, the input data may come from field study or satellite images, such as orientations points including dip and strike and horizon traces, but also seismic picks.

2.2. Defining new boundary conditions

The implicit horizon is not a mesh interface, so that no node corresponds to the intersection between the geologic surface and the 3D model. Consequently, the standard boundary conditions must be adapted to implicit horizons. The conditions are transferred to the closest neighboring tetrahedral mesh nodes. Note that a similar approach has been successfully applied to animating the

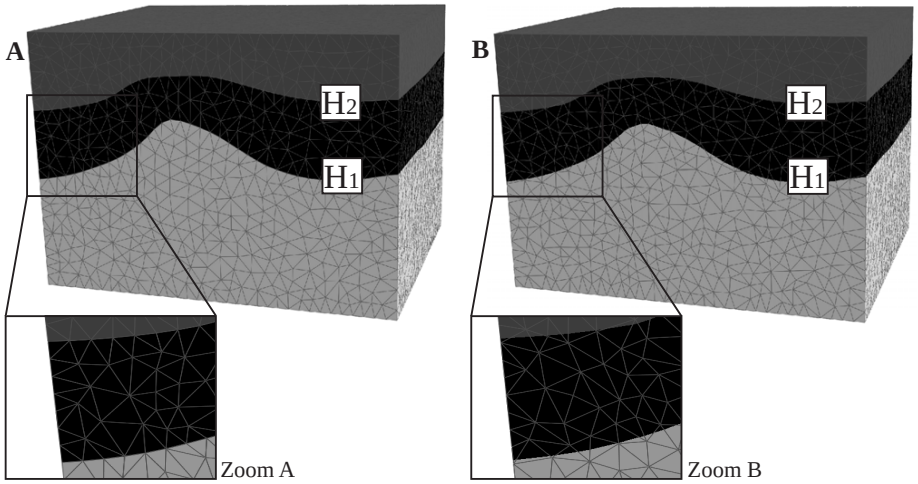

Figure 4: The implicit horizon is noted with I on the figure. The zoomed in region shows the associated distance of the nodes to the implicit surface.

simulation of deformable objects in computer graphics (Bargteil et al., 2007), although with stress boundary conditions only.

Finding the neighboring nodes

The restoration boundary condition is applied to the mesh nodes that are closest to the implicit surface to be restored, represented by a property isovalue (Fig. 4, Algo. 3 in Appendix A). For each node, the distance to the surface is computed. In practice, the nodes are found simply by comparing the values of the property on edge extremities, and the shortest distance to the implicit horizon is computed (Fig. 5, Algo. 4 in Appendix A).

Fixing the target

The aim of this boundary condition is to fix the reference elevation of the topmost horizon of the layer to restore. The neighboring nodes N should be at the same distance $d(n)$ from the implicit surface in both the restored and the deformed states. Then, the target corresponds to the reference elevation Z_r, corrected with the distance $d(n)$ between the horizon and the mesh:

$$Z(n) = Zr + d(n)$$

Where $Z(n)$ is the elevation of a node n in the restored state.

Fixing the pin regions

To have a well-posed finite element problem, a pin point, line, wall or/and block must be set on the 3D model. These conditions fix the coordinates of the considered points along some specified axis. As for the target, it is a Dirichlet boundary condition with variable values:

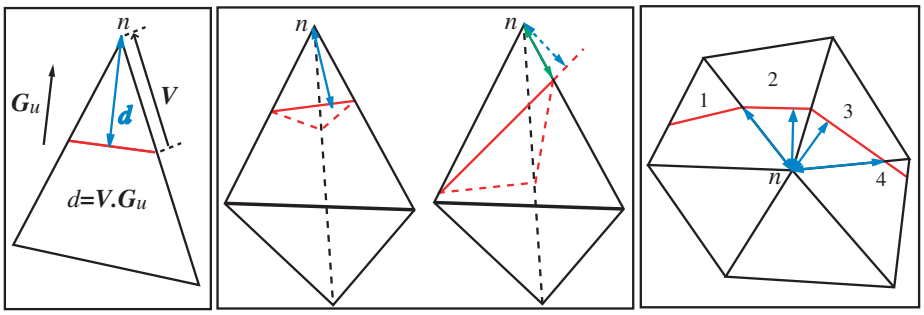

Figure 5: Computation of the shortest distance between an implicit surface (in red) and the mesh: a- Compute the dot product of the unit gradient G of the property and V, a vector from n to the intersection point on one edge, resulting in the signed distance d, between the implicit horizon and n; b)Two cases: (1) if the projected point is inside the tetrahedron, then the distance is kept; (2) if the projected point is outside (blue arrow), the distance is replaced by the shortest intersected edge (green arrow); c)The distances are computed for all the intersected tetrahedra around the considered node n, and the shortest one is kept (here it corresponds to tetrahedron 2).

$$X_i(n) = x_i(n) + d(n)$$

Where x_i is the i^{th} coordinate of the node n to be fixed ($i = \{1, 2, 3\}$), X_i its coordinate in the restored state and d the distance between the node and the implicit surface.

2.3. Setting the rock properties

Once the boundary conditions are set, we must specify the material properties per geologic sequence. There is no specific 3D region corresponding to layers, since the horizons are not mesh interfaces. To solve this issue, we set a material property M_a on the tetrahedra located completely above the considered stratigraphic or sedimentary boundary, a material property M_u on the underlying tetrahedra, and a new material on the intersected tetrahedra. This new material is approximated using a volume based proportion between the two materials M_a and M_u, as done by Bargteil et al. (2007):

$$M = \frac{V_a \cdot M_a + V_u \cdot M_u}{V_a + V_u} \tag{2}$$

V_a and V_u correspond to the volume of the intersected tetrahedra (Fig. 6).

A very elastic rheology is set in the overlying regions to emulate the absence of layers above the horizon to restore. The material is given a rubber-like rheology with a Poisson coefficient of 0.5 and a Young modulus of 0.2 GPa. In practice, the number of intersected tetrahedra is very important, and it takes a very long time to assign each tetrahedron a new material. Therefore, a limited set of materials may be defined by precomputing several materials based on volume proportion ranges:

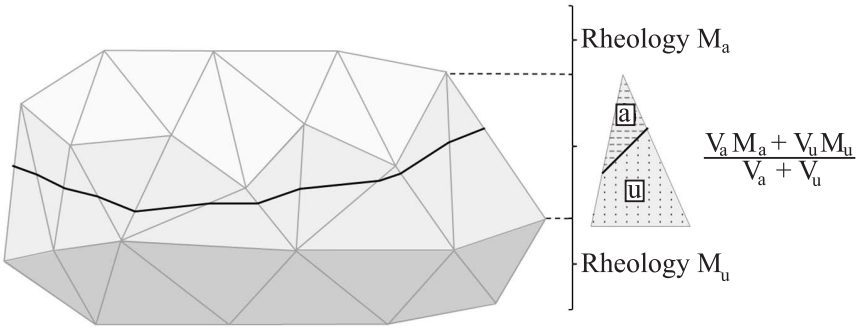

Figure 6: A rheology M_a is set above the implicit surface (in black), a material M_u under, and for the intersected tetrahedra, a volume-based percentage of the two materials above and under the surface is computed, as shown on the right.

$\frac{V_a}{V_a + V_u}$	$0 - 0.1$	$0.1 - 0.3$	$0.3 - 0.5$	$0.5 - 0.7$	$0.9 - 0.7$	$0.9 - 1$
Assigned material	M_u	$0.2M_a$ $+0.8M_u$	$0.4M_a$ $+0.6M_u$	$0.6M_a$ $+0.4M_u$	$0.8M_a$ $+0.2M_u$	M_a

3. Application to backstripping and comparison of methods

The explicit approach has been successfully applied to complex structural models, leading to consistent results (Guzofski et al., 2009; Plesch et al., 2007). To test the validity of our new approach, we propose a comparison with the explicit approach. A test case with two folded layers that was created using sub-surface geologic data (Guzofski, 2007; Müller et al., 2005) has been restored using both implicit and explicit approaches, and the results in terms of dilation have been compared.

3.1. Model building

In the explicit method, the horizons are included in the 3D model as mesh interfaces in the structural model, whereas in the implicit approach, the tetrahedral mesh is not conformable to the horizons, which are represented with property scalar fields, computed in the model (Fig. 7). For comparison purposes, both models are built with an equivalent number of tetrahedra, even if the implicit approach would allow for a lower resolution, hence faster computations.

3.2. Backstripping

The two models have been restored sequentially using the same pin wall and setting the reference horizon to zero for each horizon (Fig. 8). In the explicit case, once the first horizon is restored, the topmost sequence is removed. Then, boundary conditions are set on the second layer to be restored and flattening is performed. In the implicit case, once the first horizon is restored, a rubber

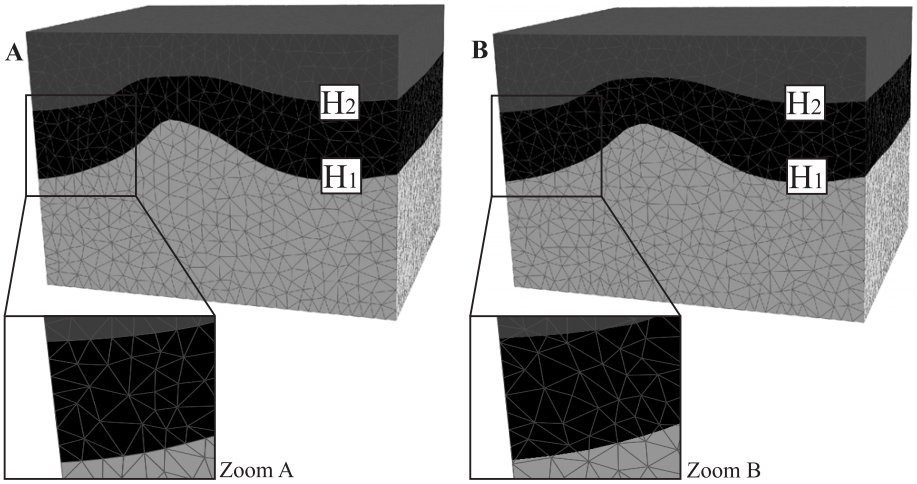

Figure 7: A) the explicit 3D model conforms the two horizons H_1 and H_2 (57 862 tetrahedra). B) the implicit model displays a stratigraphic property constrained to the two horizons and extrapolated in the 3D model. The two horizons are thus corresponding to isovalues of this property: H_1 is reprented by the -10 iso-surface, and H_2 by the 0 iso-surface (57 064 tetrahedra)

rheology is set on the formerly restored sequence and a volume based percentage material is set on the intersected tetrahedra (Eq. 2).

The performance in terms of computational time are the same for both methods: setting the boundary conditions and solving the systems with the finite element method is as fast with the explicit method as with the implicit one. However, model building requires much less interaction time in the implicit case than in the explicit case, because meshing constraints are much more flexible.

3.3. Comparison of the restored models

Method

We have considered the global volumes, V_e and V_i, and the distribution of local dilations d_e and d_i, on the explicit and implicit models. Three restoration steps have been defined: (0) is the initial stage, (1) the restored model after unfolding of the first sequence, and (2) after unfolding of the second sequence. We define the relative difference $\Delta f^{(j)}$ at step j, with $j = \{0, 1, 2\}$, $f = \{V, d\}$ as:

$$\Delta f^{(j)} = \frac{f_i^{(j)} - f_e^{(j)}}{f_i^{(j)}}$$

i corresponds to the implicit approach and e to the explicit approach.

Numbers

The following table presents the values of Δf at the different steps of restoration $\{0, 1, 2\}$, for the volume V and the dilation d:

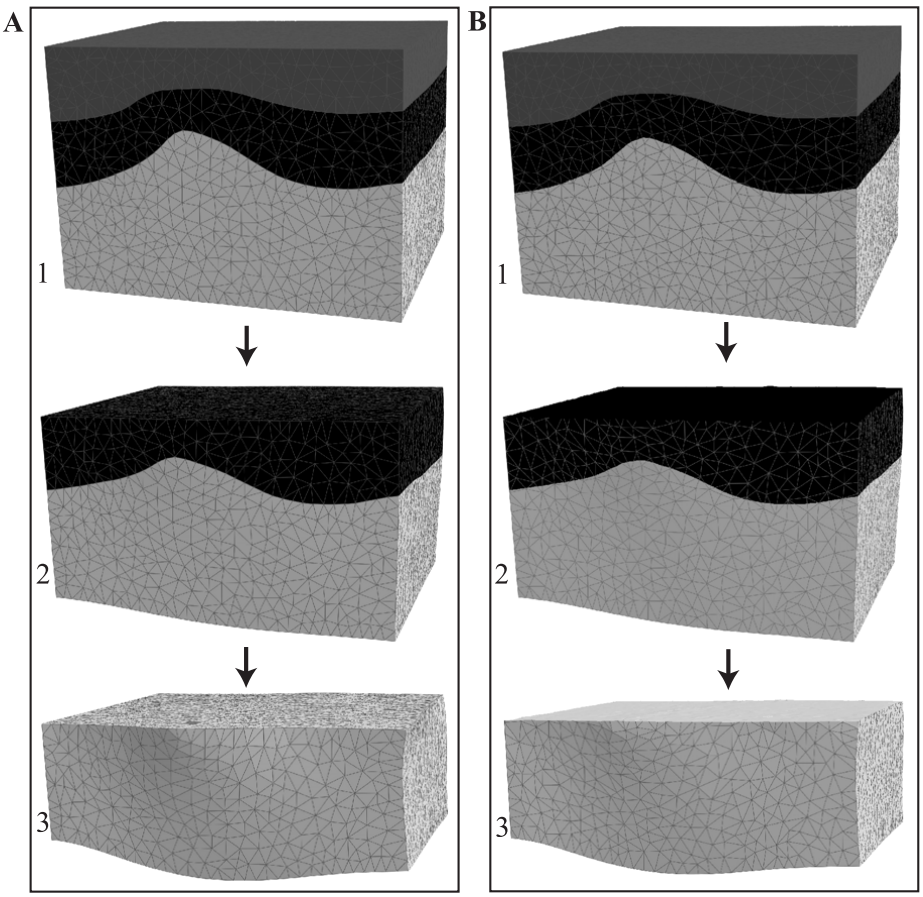

Figure 8: 1 is the initial model and 2 and 3 show the two stages of restoration. A shows an explicit restoration application. The restored topmost sequence is removed before restoring the next one. B shows an implicit restoration application, on the same 3D model. A hyper-elastic (rubber) rheology is set to the restored sequence before restoring the next one. Once a layer has been restored, all the overburden is fully transparent for better visualization.

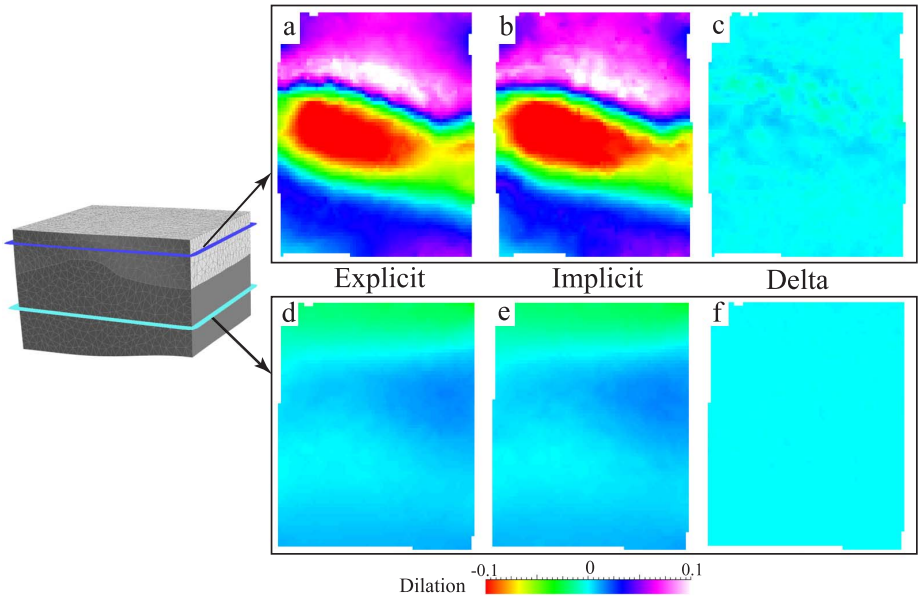

Figure 9: The retro-dilation has been transferred onto a Cartesian grid for comparison, and Δd is computed (c and f). On top is a slice of the topmost restored sequence that displays dilation calculated using the explicit and implicit methods, and difference of dilation between the methods (Δd); On bottom is a slice of the lower sequence displaying explicit, implicit and Δ dilation.

f \ j	0	1	2
V	0%	0.02%	-1.31%
d	0%	0.01%	0.12%

As shown in the table of Δf, the relative errors between explicit and implicit methods are all less than 1.5%. The slices presented in figure 9 show that variations in the model are very small. Nevertheless, the restored surface itself presents more important variations (Fig. 10), and shows that the dilation tends to be smoothed with the implicit method. However, a quantile-quantile-plot has been computed for identifying differences between the distribution of dilation d_e and d_i and shows that both implicit and explicit distributions are very well correlated (Fig. 11). These comparisons have also been performed on the second restored layer and show the same trends.

Discussion on the reasons for the differences

The observed variations between the results of both explicit and implicit methods can be explained by different phenomena:

1. The discretization may cause local variations observed in the implicitly computed dilation: the slice does not correspond to tetrahedra faces, so

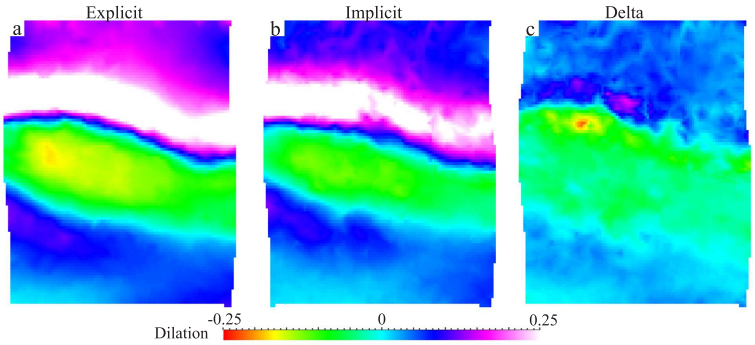

Figure 10: The two properties of retro-dilation for the top surface of the restored model, computed from the explicit method (a) and from the implicit method (b) have been transferred onto a Cartesian grid for comparison, and a new property is computed as Δ dilation (c).

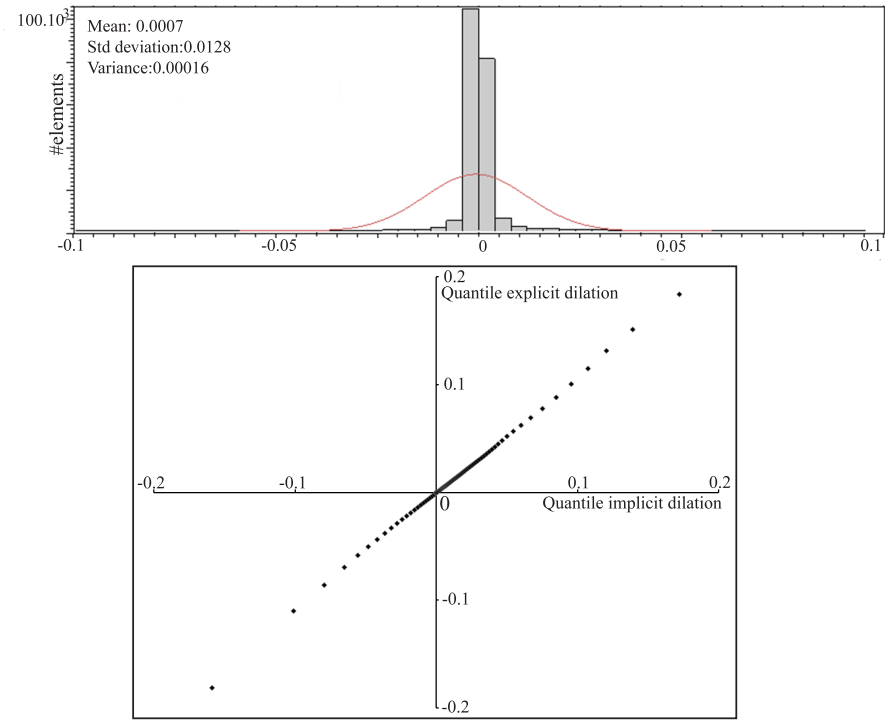

Figure 11: On top: Histogram and statistics of the property corresponding to the difference between the implicit and the explicit dilations; on bottom: quantile-quantile plot of explicit and implicit dilation

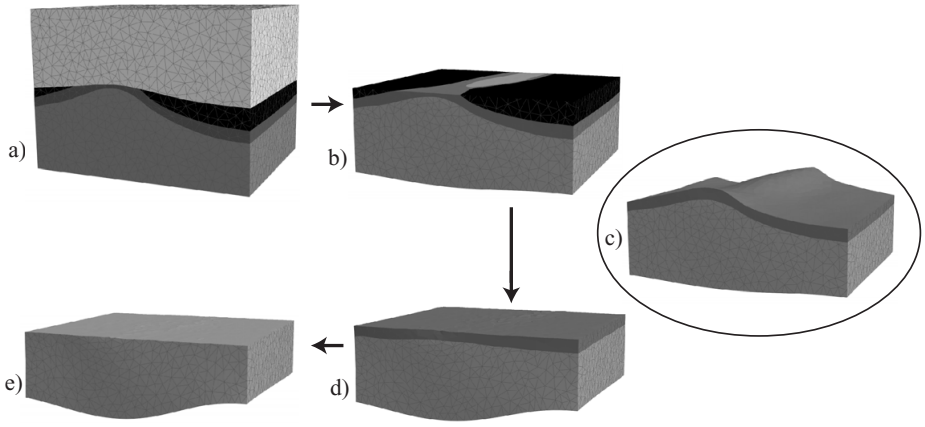

Figure 12: a) is the initial 3D model; b) is the model after the erosive layer has been restored. c) shows non-eroded layers emulated with the property of the surface which is continuous throught the anticline. d) and e) are the sequential restoration of these two layers.

the displayed dilation is an interpolated property which is not continuous through the tetrahedra. Indeed, the quantile-quantile-plot shows that the distribution of dilation properties for both explicit and implicit restorations are very well correlated, for both restored layers.

2. The approximation of the material in the tetrahedra around the restored horizon may lead to small errors in the estimation of strain located under this surface.
3. The local projections made to apply the boundary conditions may introduce errors, especially in very coarse meshes.
4. Considering the Saint-Venant's principle (published in 1855 and referred to in Love (1927)), it is not appropriate in finite element method to study the zone where the constraints are set, for edge effects may introduce artefacts. Some of the differences on the topmost restored horizon on both models may thus be due to these edge effects.

Nevertheless, we consider these differences as marginal when it comes to testing the consistency of a structural model: the localisation of the strain is very important, but the values are poorly known, so such a small difference should not bias the interpretation results.

4. Dealing with unconformities

The handling of unconformities is an issue for restoration, both for meshing (Fig. 3), and evaluating the amount of eroded material. The implicit approach (Frank et al., 2007) is useful in resolving these issues. Indeed, the implicit approach does not explicitly use continuous horizons; for erosion surfaces, a continuous horizon can be extrapolated from the eroded one following data-driven trends, making restoration possible (Fig. 12). Naturally, this eroded

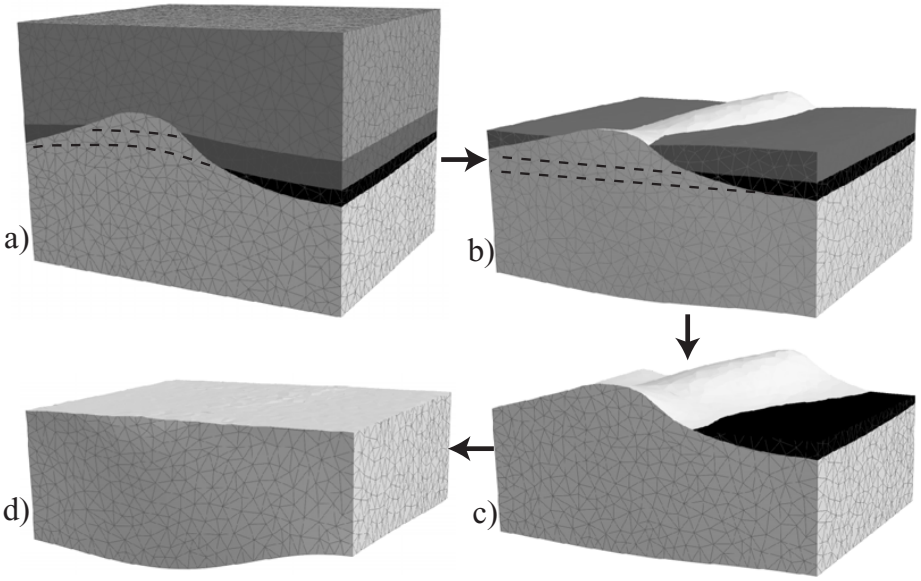

Figure 13: a) is the initial 3D structural model, including onlaps; the property corresponding to the onlapping layers are continuous, as figured for the topmost one; b) is the model after the topmost onlapping layer is restored; the continuity of the property corresponding to the second layer is figured; c) this layer is restored; d) the last layer is restored.

geometry should be questioned and possibly modified to fit interpretations, but the use of implicit surfaces is certainly a step towards an easier estimation of how much material has been eroded. In the case of onlaps, the non-deposition on the onlap surface can be emulated by the horizon property, and the restoration can thus be performed (Fig. 13). An application to the Annot syncline model (SE France, modeled by Salles et al. (2007)) has been perfomed (Fig. 14), including several layers that are onlapping onto a surface. As seen on Fig. 14, the restoration shows a progressive migration of the onlaps and a migration through time of the depocenter towards the west. It also highlights a migration of the fold hinge (current one is W and during restoration it becomes more E). This restoration allows having real thickness maps, and the restored surfaces may be used as input to forward basin modeling codes (Teles et al., 2009).

Conclusions

Volume restoration aims at sequentially unfolding the structural model, represented by a tetrahedralized and topologically consistent solid. The restoration problem is considered as a geomechanical problem, assuming a isotropic elastic rock material. This strong assumption may be discussed, since these rheological properties are not appropriate to any type of rocks. In the case of growth strata, this method nevertheless makes the elastic simplification reasonable, for it can

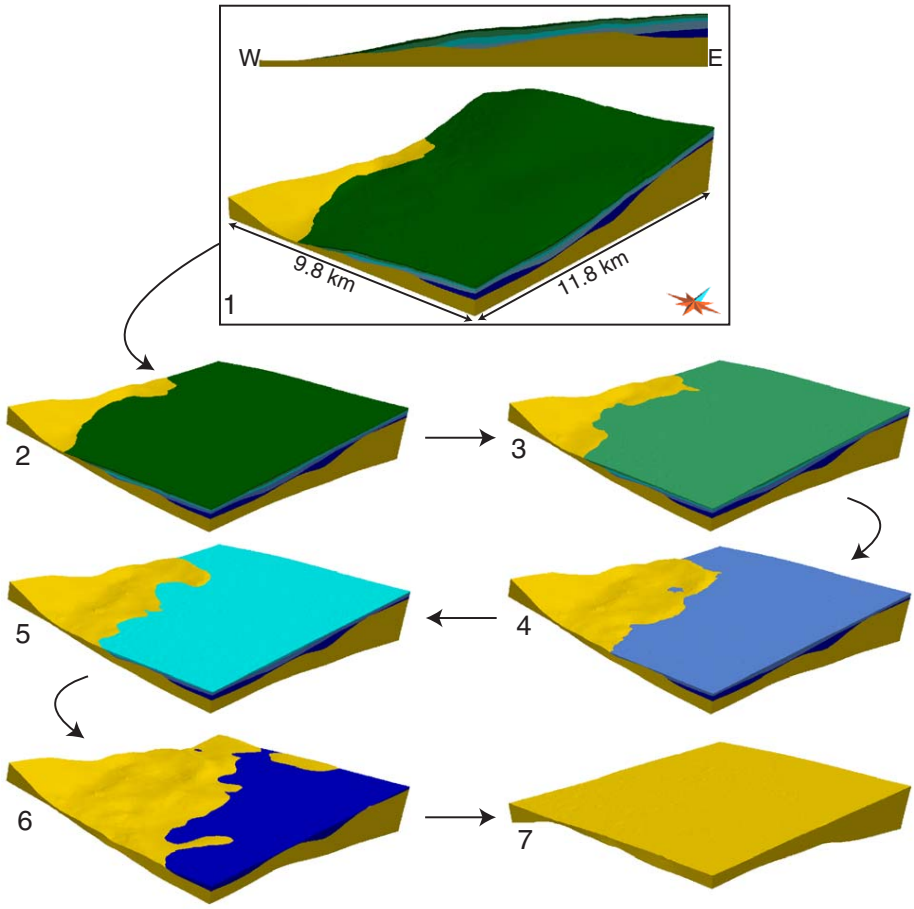

Figure 14: 1) is the initial 3D model of the Annot syncline, showing the onlapping surfaces (Salles et al., 2007). 2) is the topmost restored surface; 3) to 7) show the next restored surfaces. The restoration shows the rotation of the underlying layer (in yellow) during the deposition of the onlapping layers.

be applied sequentially to very close horizons (Guzofski et al., 2009). Future works will focus on the definition of new materials for restoration, such as transverse isotropic behaviour material to better reflect mechanical heterogeneity. Until today, the applicability of 3D restoration used to be very reduced in case of complex structural models. Indeed, a major bottleneck is the conformable mesh generation, a time-consuming step. Our new implicit restoration approach has been developed to address this problem. The horizons are now represented as stratigraphic property isovalues instead of mesh interfaces. For that, new boundary conditions have been defined. Our tests have shown that explicit and implicit methods lead to similar results, in terms of computational time and in terms of resolved strain, but model building requires much less interaction time in the implicit case. Moreover, the new approach allows the restoration of models that include unconformities such as erosion or onlap surfaces, in a way that may be more robust than the explicit method.

Acknowledgements

This research work was performed in the frame of the G◯CAD research project. Chevron and the other companies and Universites of the G◯CAD Consortium are hereby acknowledged for financial support. Lise Salles provided the Annot model. We would like to thank Eric de Kemp and Richard J. Lisle for their constructive reviews, and Chris Guzofski for his active early reading. Thanks to Thomas Viard for the visualization tools. This is CRPG contribution number 1991.

References

Bargteil, A. W., Wojtan, C., Hodgins, J. K., Turk, G., 2007. A finite element method for animating large viscoplastic flow. ACM Transactions on Graphics 26 (3).

Calcagno, P., Chilès, J., Courrioux, G., Guillen, A., 2008. Geological modelling from field data and geological knowledge part I. Modelling method coupling 3D potential-field interpolation and geological rules. Physics of the Earth and Planetary Interiors 171 (1-4), 147–157.

Caumon, G., Antoine, C., Tertois, A.-L., 2007. Building 3D geological surfaces from field data using implicit surfaces. 27th GOCAD Meeting, Nancy, France.

Chamberlin, R., 1910. The appalachian folds of central pennsylvania. Journal of Geology 18, 228–251.

Charlez, P., 1991. Rocks Mechanics : Theoretical Fundamentals. Editions Technip.

Dahlstrom, C. D. A., 1969. Balanced cross sections. Canadian Journal of Earth Sciences (6), 743–757.

De Santi, M., Campos, J., Martha, L., 2002. A finite element approach for geological section reconstruction. 22^{th} Gocad Meeting, Nancy, June 2002.

De Santi, M. R., Campos, J. L. E., Martha, L. F., 2003. 3D geological restoration using a finite element approach. 23th GOCAD Meeting, Nancy, France.

Doyen, P., 2007. Seismic Reservoir Characterization, An Earth Modeling Perspective. EAGE.

Dunbar, J., Cook, R., 2003. Palinspastic reconstruction of structure maps: an automated finite element approach with heterogeneous strain. Journal of Structural Geology 26, 1021–1036.

Frank, T., Tertois, A.-L., Mallet, J.-L., 2007. 3D reconstruction of complex geological interfaces from irregularly distributed and noisy point data. Computer and Geosciences 33 (7), 932, 943.

Gibbs, A., 1983. Balanced cross section construction from seismic sections in areas of extensional tectonics. Journal of Structural Geology 5 (2), 153–160.

Gratier, J. P., Guillier, B., 1993. Compatibility constraints on folded and faulted strata and calculation of total displacement using computational restoration (unfold program). Journal of Structural Geology 15 (3-5), 391–402.

Groshong, R., 1999. 3d Structural Geology: A Practical Guide To Surface And Subsurface Map Interpretation. Springer Verlag, Ch. 11: Structural validation, restoration and prediction, p. 400.

Guzofski, C., 2007. Mechanics of fault-related folds and critical taper wedges. Ph.D. thesis, Harvard University, Cambridge, USA.

Guzofski, C., Mueller, J., Shaw, J., Muron, P., Medwedeff, D., Bilotti, F., Rivero, C., 2009. Insights into the mechanisms of fault-related folding provided by volumetric structural restorations using spatially varying mechanical constraints. AAPG Bulletin 93, 479–502.

Hugues, T., 1987. The Finite Element Method : Linear Static and Dynamic Finite Element Analysis. Prentice-Hall.

Jacquemin, P., 1999. Balanced unfolding : removing gaps between horizons and faults. In 19^{nd} Gocad Meeting Report, Nancy.

Lepage, F., 2002. Triangle and tetrahedral meshes for geological models. In 22^{nd} Gocad Meeting Report, Nancy.

Lo, S., 2002. Finite element mesh generation and adaptive meshing. Progress in Structural Engineering and Materials 4, 381, 399.

Love, A., 1927. A Treatise on the Mathematical Theory of Elasticity. Cambridge University Press.

Maerten, L., Maerten, F., 2006. Chronologic modeling of faulted and fractured reservoirs using geomechanically based restoration: Technique and industry applications. AAPG Bulletin 90 (8), 1201, 1226.

Mallet, J.-L., 1992. Discrete smooth interpolation. Computer-Aided Design 24 (4), 263–270.

Mallet, J.-L., 2002. Geomodeling. Oxford University Press First edition.

Mallet, J.-L., 2004. Space-Time Mathematical Framework for Sedimentary Geology. Mathematical Geology 36 (1), 1–32.

Massot, J., 2002. Implémentation de méthodes de restauration équilibrée 3D. Ph.D. thesis, INPL, Nancy, France.

Moretti, I., 2008. Working in complex areas: New restoration workflow based on quality control, 2D and 3D restorations. Marine and Petroleum Geology 25, 202–218.

Moretti, I., Lepage, F., Guiton, M., 2006. Kine3D: a new 3D restoration method based on a mixed approach linking geometry and geomechanics. Oil & Gas Science and Technology 61 (2), 277–289.

Moyen, R., Mallet, J.-L., Frank, T., Leflon, B., Royer, J.-J., 2004. 3D-parameterization of the 3D geological space - the GeoChron model. In: Proc. European Conference on the Mathematics of Oil Recovery (ECMOR IX). A004 , 8p.

Müller, J., Guzofski, C., Rivero, C., Plesch, A., Shaw, J., Bilotti, F., Medwedeff, D., 2005. New approaches to 3D structural restoration in fold-and-thrust belts using growth data. AAPG Annual Convention, Calgary, Canada.

Muron, P., 2005. Méthode numériques 3D de restauration des structures géologiques faillées. Ph.D. thesis, Institut Polytechnique National de Lorraine.

Muron, P., Mallet, J.-L., 2003. 3D balanced unfolding: the tetrahedral approach. 23th GOCAD Meeting, Nancy, France.

Owen, S., 1998. A survey of unstructured mesh generation technology. 7th International Meshing Roundtable, Dearborn, MI.

Plesch, A., Shaw, J. H., Kronman, D., 2007. Mechanics of low-relief detachment folding in the bajiaochang field, sichuan basin, china. AAPG Bulletin 91, 1559–1575.

Rouby, D., 1994. Restauration en carte des domaines faillés en extension. Ph.D. thesis, Université de Rennes I, mémoires Géosciences Rennes No 58.

Rouby, D., Xiao, H., Suppe, J., 2000. 3-D restoration of complexly folded and faulted surfaces using multiple unfolding mechanisms. AAPG Bulletin 84 (6), 805–829.

Salencon, J., 2000. Mécanique des Milieux Continus. Tome I: Concepts Généraux. Editions de l'école Polytechnique.

Salles, L., Ford, M., LeSolleuz, A., Joseph, P., de Veslud, C. L. C., 2007. 3D structural control of turbidite deposition in a foreland fold and thrust belt: the Annot sandstone depocentre of Sanguinière, SE France. AAPG Annual Meeting, Long Beach, California.

Sheider, F., Potdevin, J., Wolf, S., Faille, I., 1996. Mechanical and chemical compaction model for sedimentary basin simulators. Tectonophysics 263, 307–317.

Teles, V., Joseph, P., Salles, L., Bacq, M. L., Maktouf, F., 2009. Simulation of the annot turbidite system with the cats process-based numerical model. AAPG Annual Convention, Denver, USA.

Thibert, B., Gratier, J.-P., Morvan, J.-M., 2005. A direct method for modeling developable strata and its geological application to Ventura Basin (California). Journal of Structural Geology 27, 303–316.

Titeux, M.-O., Royer, J.-J., 2008. Upscaling mechanical properties in layered geological formations. 28th GOCAD Meeting, Nancy, France.

Wriggers, P., 2000. Computational Contact Mechanics. Wiley.

Zienkiewicz, O., 1977. The Finite Element Method, 3rd Edition. McGraw-Hill.

Zienkiewicz, O., Taylor, R., 2000a. The Finite Element Method - Volume I: The Basis, 5th Edition. Butterworth-Heinemann.

Zienkiewicz, O., Taylor, R., 2000b. The Finite Element Method - Volume II: Solid mechanics. Butterworth-Heinemann.

A. Boundary conditions algorithms

Algorithm 1 Restores the reference horizon

Input: The topmost horizon H to restore, the reference elevation Z_r

1: Z corresponds to the restored configuration
2: **for** Each node $n \in H$ **do**
3: $\quad Z(n) = Z_r$
4: **end for**

Algorithm 2 Fixes the pin point, line, wall, block

Input: The axis i to fix; the region R to fix

1: x_i is the component along the axis i in the current configuration; X_i is in the restored configuration
2: **for** Each node $n \in R$ **do**
3: **for** i from 1 to 3 **do**
4: **if** i is fixed **then**
5: $X_i(n) = x_i(n)$
6: **end if**
7: **end for**
8: **end for**

Algorithm 3 Finds the neighboring nodes and stores the signed shortest distance d to the implicit surface

Input: The property P and the isovalue I representing the implicit horizon to restore; a region R containing this horizon (it can be the entire model).

Output: N: a set of nodes; $d(n), n \in N$:signed distance to the horizon

for each tetrahedron edge $e \in R$ **do**
 $\text{value}_1 \leftarrow P(n_1) - I$ and $\text{value}_2 \leftarrow P(n_2) - I$ // *n_1 and n_2 are the two extremities of the current edge*
 if $\text{value}_1 = 0$ **then**
 add n_1 to N
 $d(n) \leftarrow 0$
 else if $\text{value}_2 = 0$ **then**
 add n_2 to N
 $d(n) \leftarrow 0$
 else if $\text{value}_1 \cdot \text{value}_2 < 0$ **then**
 $Or_{sign} = \text{Sign}(\nabla P(e) \cdot (001)^T)$ // *Find whether the gradient of P on edge e is pointing upward or downward: if the two orientations are the same $Or_sign = +1$ and -1 else*
 if $\|\text{value}_1\| < \|\text{value}_2\|$ **then**
 add n_1 to N
 $d(n_1) \leftarrow Or_{sign} \cdot \text{distance}(n_1)$ // *See Algo.4*
 else
 add n_2 to N
 $d(n_2) \leftarrow Or_{sign} \cdot \text{distance}(n_2)$ // *See Algo.4*
 end if
 end if
end for

Algorithm 4 Computes the signed shortest distance d to the implicit surface

Input: The property P and the isovalue I representing the implicit horizon to restore; a node n on an edge cut by the surface

Output: Distance $d(n)$ between n and the isosurface

for Each tetrahedron T around the node n **do**
  float:cur_dist $\leftarrow V \cdot G_P(T)$ // *V is a vector along an edge of T, from n to the intersection edge-implicit surface and $\nabla P(T)$ is the unit gradient of the property P in T*
  Build $\mathbf{d}(T)$ = vector (origin=n, end=orthogonal projection of n on the implicit surface)
  if $\mathbf{d}(\mathbf{T}) \cdot \nabla P(T) < 0$ **then**
    cur_dist $\leftarrow -$cur_dist // *n is under the implicit surface*
  end if
  if $n + \mathbf{d}(T)$ is inside T **then**
    cur_dist $\leftarrow$ cur_dist // *Keep the current distance*
  else
    cur_dist $\leftarrow$ shortest intersected edge $\in T$
  end if
  if $d(n)$not initialized or cur_dist $< d(n)$ **then**
    $d(n) \leftarrow$ cur_dist
  end if
end for

Algorithm 5 Restores the implicit topmost surface

Input: N the set of neighboring nodes of the horizon to restore (Algo. 3) and the associated signed distance (Algo. 4), the reference elevation Z_r

1: **for** Each node $n \in N$ **do**
2: $Z(n) = Z_r + d(n)$ // *Z corresponds to the restored configuration*
3: **end for**

Algorithm 6 Fixes the pin point or line in an implicit approach

Input: N the set of neighboring nodes n of the region to fix (Algo. 3) and the associated signed distances $d(n)$ (Algo. 4), the axis i to fix // *Algo. 3 is applied to a region of the model to find the appropriate nodes; a 1D region will lead to a point (intersection between a line and a surface), a 2D region to a line (intersection surface-surface), and a 3D to a surface (intersection volume - surface)*

1: **for** Each node $n \in N$ **do**
2: $X_i(n) = x_i(n) + d(n)$ // *X_i and x_i correspond to coordinate along the axis i, respectively to the restored and the present states*
3: **end for**

B. Continuum mechanics applied to restoration

The formulation of restoration as a mechanical problem states that the computation of the restored configuration has to preserve the moments of the considered geological domain. This appendix presents the main measures and principles for solving a restoration problem and analyzing results, especially the deformations and geological strains.

B.1. Measures

Measures of the deformation

To locally describe the deformations processes of an elementary particle in a layer, let us introduce a second order tensor $\mathbf{F}$, commonly known as the deformation gradient, or Jacobian matrix $\mathbf{F}$:

$$\mathbf{F} = \frac{\partial \mathbf{x}}{\partial \mathbf{X}} = \begin{bmatrix} \frac{\partial x}{\partial X} & \frac{\partial x}{\partial Y} & \frac{\partial x}{\partial Z} \\ \frac{\partial y}{\partial X} & \frac{\partial y}{\partial Y} & \frac{\partial y}{\partial Z} \\ \frac{\partial z}{\partial X} & \frac{\partial z}{\partial Y} & \frac{\partial z}{\partial Z} \end{bmatrix} \tag{3}$$

$\mathbf{F}$ characterizes the transformation of an elementary segment $d\mathbf{X}$ from its current configuration to its restored configuration: $d\mathbf{x} = \mathbf{F} \cdot d\mathbf{X}$ where $d\mathbf{X}$ is an elementary vector in the deformed configuration and $d\mathbf{x}$ its image in the restored configuration. The determinant of the Jacobian matrix $\mathbf{F}$ is called the Jacobian of the transformation and has to be strictly positive to ensure the continuity of the domain.

In geology, the Green-Lagrange tensor is widely used to characterize the deformation because it is easily linearisable in small deformations (Salencon, 2000). The Green-Lagrange tensor $\mathbf{E}$ characterizes the variation of the square lengths of a material segment before and after deformation. It is directly expressed as a function of the displacement gradient:

$$\mathbf{E} = \frac{1}{2}(\mathbf{C} - 1) = \frac{1}{2}(\mathbf{F}^T\mathbf{F} - 1) = \frac{1}{2}(\nabla\mathbf{r} + (\nabla\mathbf{r})^T + \nabla\mathbf{r} \cdot (\nabla\mathbf{r})^T) \tag{4}$$

where ∇ designates the nabla operator relatively to the reference configuration, *i.e.* the present configuration, and $\mathbf{u}$ the displacement vectors from the present state to the restored state.

Small and large deformations

Most 3D restoration approaches (De Santi et al., 2003; Maerten and Maerten, 2006; Massot, 2002) are based upon the hypothesis of small deformations: the length variation of a material segment is small as compared to the length of the segment. The quadratic terms of the tensor $\mathbf{E}$ are thus neglected and the tensor of small deformations ε (linear Green-Lagrange tensor) can be defined:

$$\varepsilon = \frac{1}{2}(\nabla\mathbf{r} + (\nabla\mathbf{r})^T) \tag{5}$$

Measures of the stresses

The deformation of the geological structures is the expression of the events the medium underwent. In continuum mechanics, the mechanical actions are called stresses and are represented with torsors (a force, a moment and an application point). Two types of stresses are defined on a bound domain:

1. the exterior stresses are the mechanical actions external to the domain (e.g. gravitation, magnetic forces, regional constraints on domain boundary).
2. the interior stresses are the actions of the domain particles. They are represented with a second order tensor σ called Cauchy constraints tensor. It allows us to define the surface density of force $\mathbf{t}$ applied to a face with a unit normal $\mathbf{n}$:

$$\sigma \cdot \mathbf{n} = \mathbf{t} d\Gamma \tag{6}$$

where Γ is the domain boundary.

Several other stress tensors exist, for example the first tensor of Piola-Kirchhoff, allowing to compute the Cauchy contraint on a face with a normal $\mathbf{n}_0$ in its current configuration:

$$\mathbf{P} \cdot \mathbf{n}_0 = \mathbf{t}_0 d\Gamma_0 \mathbf{S} \cdot \mathbf{n}_0 = \mathbf{F}^{-1} \cdot \mathbf{t}_0 d\Gamma_0 \tag{7}$$

Where the index 0 refers to the present configuration.

B.2. Fundamental conservation laws

The fundamental equations controlling the motions, deformations, and stresses in the continous media come directly from conservation laws. If we consider the geological structures as bounded mechanical systems, four conservation laws are relevant (Salencon, 2000): the conservation of mass, linear momentum, energy and angular momentum. In restoration, only the two first laws are considered (Maerten and Maerten, 2006; Moretti et al., 2006; Muron, 2005).

Conservation of mass

We consider there is no particle flow through the borders of the geological domain, so the mass of the domain must be constant during the transformation. The equation of conservation of mass has two major terms: one of density variation ($\frac{\partial \rho}{\partial t}$ where ρ is the density), and one of material flow on the borders of the domain ($\rho \nabla \cdot \mathbf{v}$ where $\mathbf{v}$ is the velocity field):

$$\frac{\partial \rho}{\partial t} + \rho \nabla \cdot \mathbf{v} = 0 \tag{8}$$

If we neglect the variations of density, this principle can be turned into the preservation of volume, also used in geometrical restoration (Mallet, 2002; Massot, 2002).

Conservation of linear momentum

The conservation of linear momentum is equivalent to Newton's second law, relating external forces acting on a material domain and its acceleration. The external forces considered here are of two types: the volume forces ($\rho\hat{\mathbf{b}}$) and the forces of surfaces transformed by Gauss theorem ($\nabla \cdot \sigma$):

$$\rho\frac{\partial \mathbf{v}}{\partial t} - \rho\hat{\mathbf{b}} - \nabla \cdot \sigma = 0 \tag{9}$$